Durham University

Durham Research Online

Deposited in DRO:

21 May 2019

Version of attached file:

Accepted Version

Peer-review status of attached file:

Peer-reviewed

Citation for published item:

Mendis, B.G. (2019) 'Planck's generalised radiation law and its implications for cathodoluminescence spectra.', Ultramicroscopy., 204 . pp. 73-80.

Further information on publisher's website:

https://doi.org/10.1016/j.ultramic.2019.05.007

Publisher's copyright statement:

© 2019 This manuscript version is made available under the CC-BY-NC-ND 4.0 license
http://creativecommons.org/licenses/by-nc-nd/4.0/

Additional information:

Use policy

The full-text may be used and/or reproduced, and given to third parties in any format or medium, without prior permission or charge, for personal research or study, educational, or not-for-profit purposes provided that:

- a full bibliographic reference is made to the original source
- a link is made to the metadata record in DRO
- the full-text is not changed in any way

The full-text must not be sold in any format or medium without the formal permission of the copyright holders.

Please consult the full DRO policy for further details.

Durham University Library, Stockton Road, Durham DH1 3LY, United Kingdom
Tel : +44 (0)191 334 3042 | Fax : +44 (0)191 334 2971
https://dro.dur.ac.uk

Planck's generalised radiation law and its implications for cathodoluminescence spectra

BG Mendis

Dept of Physics, Durham University, Durham, DH1 3LE, UK

Abstract

Cathodoluminescence (CL) is an important analytical technique for probing the optical properties of materials at high spatial resolution. Interpretation of CL spectra is however complicated by the fact that the spectrum depends on the carrier injection density of the incident electron beam. Here a generalised version of Planck's radiation law is used to uncover the evolution of CL spectra with injection under steady-state conditions. The importance of the quasi-Fermi level is highlighted and it is shown that steady-state luminescence is suppressed when the carrier distributions undergo a population inversion. The theory is consistent with some well-known luminescence phenomena, such as the blue shifting of donor-acceptor pair transitions with increased injection, and its predictions are experimentally verified on CdTe and GaN, which are exemplar thin-film solar cell and light emitting diode materials respectively. Furthermore, the discussion is broadened to include pulsed illumination in time resolved CL, where the carrier distribution is dynamically evolving with time.

Keywords: cathodoluminescence, Planck's radiation law, band edge luminescence, donor-acceptor pair transition.

1. Introduction

Cathodoluminescence (CL) is a highly versatile electron microscopy technique for analysing the optical properties of inorganic semiconductors [1-2] as well as plasmonics [3-4]. The incoherent luminescence produced by electron-hole pair recombination provides important information on the electrical activity of defects, such as grain boundaries [5-8], as well as doping heterogeneities [9-11]. Furthermore, the development of time resolved CL at high spatial and temporal resolution by pulsed laser excitation of a photocathode [12-13] has enabled carrier lifetime measurement in localised regions of the specimen [14-15]. Due to the nature of the recombination process the CL spectrum is sensitive to the carrier injection density of the electron beam as well as the temperature of the specimen, which can be cryogenically cooled in order to increase the radiative recombination efficiency. Ideally both the temperature and injection density should be similar to the operating conditions of the device (e.g. solar cell, light emitting diode) for which the semiconductor is intended. Electron-hole pair generation by the incident electron beam is however inherently non-uniform within the specimen and once generated the carriers can undergo drift, diffusion and recombination. It is therefore often difficult to determine if the measured CL spectrum corresponds to the desired injection density, especially if the semiconductor material parameters, such as carrier diffusion length and lifetime, are not well known. This is also true for interpreting transient spectra in time resolved CL, where the injection is extremely high at short time delays but progressively decreases to low injection conditions with time.

The generalised version of Planck's radiation law describes the 'non-thermal' radiation (i.e. luminescence) emitted by a material [16-17]. The material need not be a black body and is also not required to be in thermal equilibrium with its surroundings, although it is assumed that thermal and chemical equilibrium has been achieved within the material. This means that all atomic constituents (i.e. electrons and nuclei) are at the same temperature and occupation of the valence and conduction bands are governed by their respective quasi-Fermi levels. In most 'continuous' CL measurements, where the incident electron beam illumination is practically time independent, the acquisition time for the CL spectrum is significantly longer than the carrier lifetime. The material is therefore in steady-state for Planck's generalised radiation law to be applicable. The generalised radiation law has been empirically verified on light emitting diodes [18] and solar cells [19]. Furthermore, it has been used to measure sub-band gap absorption [20-21] and probe defect levels in $Cu(In,Ga)Se_2$ based solar cell devices [22-23].

In this paper Planck's law is used to make some predictions of the CL spectrum and its evolution with electron beam injection. The derivation of the generalised radiation law for band edge luminescence, as described in [16], is modified in order to be applicable to CL experiments. The importance of the electron and hole quasi-Fermi levels on the CL spectrum is highlighted. Furthermore, the analysis is extended to include electronic transitions between discrete energy levels, such as, for example, donor-acceptor pair (DAP) luminescence [2]. The predictions are experimentally verified for CdTe and GaN, which are exemplar semiconductor materials for thin-film solar cells and light emitting diodes respectively. Finally, a comparison between time resolved, pulsed mode CL and continuous, steady-state CL is also presented.

2. Experimental Method

CL measurements were carried out on a Hitachi SU70 scanning electron microscope (SEM) at 15 keV incident beam energy. The beam current was measured using a Faraday cup and was varied through a suitable combination of objective and anode aperture sizes as well as condenser lens settings. CL spectra were recorded using a PIXIS silicon CCD camera and Gatan MonoCL system with 300 lines/mm diffraction grating. Liquid nitrogen temperature (77 K) CL spectra were acquired using a Gatan C1002 cryo-stage, which cooled the specimen by passing dry nitrogen gas through a liquid nitrogen dewar before circulating through the stage module. The spectra were acquired continuously while scanning the beam over a 21 x 21 μm area. This was done in order to average out inhomogeneities in the sample, such as dislocations, grain boundaries etc. The pixel dwell time was 0.1 seconds, which is significantly longer than the nanosecond carrier lifetime of the CdTe and GaN thin-films investigated here, so that steady-state conditions are established during acquisition. The spectra were not corrected for the non-uniform response of the instrument over the wavelength range of interest. CL spectra were also acquired from the CdTe sample at 12 K using liquid-He cooling in an Attolight 'Chronos' SEM operating at 6 kV. The field emission gun could be used in either continuous or pulsed illumination mode, the latter using a frequency doubled Ti:sapphire laser with 80 MHz repetition rate for photoemission. CL spectra were acquired from a 9 x 9 μm scanned area on a Horiba Synapse CCD camera (for pulsed illumination the CL spectrum was time integrated).

The CdTe thin-film sample was grown by close space sublimation at a temperature of 575°C. The purity of the Alfa Aesar CdTe source material was 99.999%. Following deposition the material was chlorine doped by depositing a 200 nm thick layer of $CdCl_2$ on the surface and annealing at 440°C for 20 mins in air. Further details of the deposition can be found in [24]. The as-deposited sample had a rough surface due to the underlying CdTe columnar grain structure. Argon ion-beam polishing was therefore used to prepare flat surfaces for CL. The final Ar ion-beam energy was 2 keV and had a 2° incidence angle to the sample surface. The deposition conditions for the GaN thin-film sample are unfortunately unknown. The as-received sample had a smooth surface and could therefore be analysed in the SEM without any further preparation.

3. Results and Discussion

3.1 *Generalised radiation law and the significance of quasi-Fermi levels*

The derivation of the generalised radiation law, as presented in [16] for band edge luminescence, will first be extended to include the conditions relevant for CL (specifically carrier generation by the incident electron beam must be taken into account). Consider electronic transitions between the conduction and valence bands. The photoabsorption (r_a), stimulated emission (r_{st}) and spontaneous emission (r_{sp}) rates at photon energy $\hbar\omega$ are given by [16]:

$$r_a(\hbar\omega) = n_\gamma(\hbar\omega)\int_{E_{min}}^{E_{max}} M(E,\hbar\omega)n_v(E)n_c{}'(E+\hbar\omega)dE \quad \ldots (1a)$$

$$r_{st}(\hbar\omega) = n_\gamma(\hbar\omega)\int_{E_{min}}^{E_{max}} M(E,\hbar\omega)n_v{}'(E)n_c(E+\hbar\omega)dE \quad \ldots (1b)$$

$$r_{sp}(\hbar\omega) = D_\gamma(\hbar\omega)\int_{E_{min}}^{E_{max}} M(E,\hbar\omega)n_v{}'(E)n_c(E+\hbar\omega)dE \quad \ldots (1c)$$

where n_γ is the photon density and D_γ is the photon density of states per unit energy interval. n_v, n_v' are the density of occupied and unoccupied states in the valence band respectively and similarly for n_c, n_c' and the conduction band. $M(E,\hbar\omega)$ is a photon transition matrix element. Integration is carried out over the valence band energy range [E_{min}, E_{max}].

In a CL experiment the electron-hole pair generation rate (r_e) due to the incident electron beam is also important:

$$r_e(\hbar\omega) = \int_{E_{min}}^{E_{max}} L(E,\hbar\omega)n_v(E)n_c{}'(E+\hbar\omega)dE \quad \ldots (2)$$

The modified transition matrix element L is determined by noting that the transition rate r_e between an occupied valence band state of energy E and unoccupied conduction band state of energy $(E+\hbar\omega)$ can also be expressed as $(j_e\sigma_e v_e)n_v(E)n_c'(E+\hbar\omega)$, where j_e is the incident electron flux, σ_e is the inelastic scattering cross-section and v_e is the incident electron speed ($\sigma_e v_e$ is the scattering volume per unit time). Using the expression for the inelastic cross-section [25]:

$$L(E,\hbar\omega) = j_e\sigma_e v_e = j_e v_e \left(\frac{1}{2\pi^2 a_o}\right)^2 \left(\frac{k_m}{k_0}\right) \int \frac{|\varepsilon(\mathbf{q})|^2}{q^4} d\Omega \qquad \ldots (3)$$

where a_o is the Bohr radius, (k_0, k_m) are the wave numbers for the incident and inelastic scattered electron respectively, $\mathbf{q}$ is the scattering vector and Ω is the solid angle. The electron transition matrix element $\varepsilon(\mathbf{q})$ is given by [25]:

$$\varepsilon(\mathbf{q}) = \sum_{\alpha} \left\langle u_f \middle| \exp(-2\pi i \mathbf{q}\cdot\mathbf{r}_\alpha) \middle| u_i \right\rangle \qquad \ldots (4)$$

where (u_i, u_f) are the initial and final state specimen electron wavefunctions respectively and $\mathbf{r}_\alpha$ is the position vector of the α^{th}-specimen electron.

At steady-state the rates for upward and downward electronic transitions must be equal, i.e.:

$$r_a(\hbar\omega) + r_e(\hbar\omega) = r_{sp}(\hbar\omega) + r_{st}(\hbar\omega) + r_{\text{Auger}}(\hbar\omega) \qquad \ldots (5)$$

where the Auger recombination rate, r_{Auger}, is included here for completeness, but is otherwise negligible for a direct band gap semiconductor under low injection conditions. Ignoring r_{Auger} and solving Equation (5) for n_γ gives:

$$n_\gamma(\hbar\omega) = \frac{D_\gamma(\hbar\omega)\int_{E_{min}}^{E_{max}} M(E,\hbar\omega)n_v'(E)n_c(E+\hbar\omega)dE}{\int_{E_{min}}^{E_{max}} M(E,\hbar\omega)n_v'(E)n_c(E+\hbar\omega)\left[\frac{n_v(E)n_c'(E+\hbar\omega)}{n_v'(E)n_c(E+\hbar\omega)} - 1\right]dE} - \frac{\int_{E_{min}}^{E_{max}} L(E,\hbar\omega)n_v(E)n_c'(E+\hbar\omega)dE}{\int_{E_{min}}^{E_{max}} M(E,\hbar\omega)n_v(E)n_c'(E+\hbar\omega)\left[1 - \frac{n_v'(E)n_c(E+\hbar\omega)}{n_v(E)n_c'(E+\hbar\omega)}\right]dE} \qquad \ldots (6)$$

From semiconductor theory $n_v(E) = D_v(E)f(E)$ and $n_v'(E) = D_v(E)[1-f(E)]$, where $D_v(E)$ is the electronic density of states for the valence band and $f(E) = 1/\{1+\exp[(E-E_{Fp})/kT]\}$ is the Fermi-Dirac distribution function, with E_{Fp} being the hole quasi-Fermi energy level [26]. Equivalent expressions can be written for $n_c(E)$ and $n_c'(E)$. These relationships are used to simplify the square bracket terms within the denominator of Equation (6), i.e.:

$$\frac{n_v(E)n_c{}'(E+\hbar\omega)}{n_v{}'(E)n_c(E+\hbar\omega)} - 1 = \exp\left(\frac{\hbar\omega-\mu_\gamma}{kT}\right) - 1 \quad \ldots (7a)$$

$$1 - \frac{n_v'(E)n_c(E+\hbar\omega)}{n_v(E)n_c'(E+\hbar\omega)} = 1 - \exp\left(\frac{\mu_\gamma-\hbar\omega}{kT}\right) \quad \ldots (7b)$$

where $\mu_\gamma = E_{Fn} - E_{Fp}$ is the electron (E_{Fn}) and hole (E_{Fp}) quasi-Fermi level splitting and kT has its usual meaning. Equation (6) then simplifies to:

$$n_\gamma(\hbar\omega) = \frac{D_\gamma(\hbar\omega)}{\exp\left(\frac{\hbar\omega-\mu_\gamma}{kT}\right)-1} + \frac{Q(\hbar\omega)}{\exp\left(\frac{\mu_\gamma-\hbar\omega}{kT}\right)-1} = n_\gamma^{\max}(\hbar\omega) + \frac{Q(\hbar\omega)}{\exp\left(\frac{\mu_\gamma-\hbar\omega}{kT}\right)-1} \quad \ldots (8)$$

$$Q(\hbar\omega) = \frac{\int_{E_{min}}^{E_{max}} L(E,\hbar\omega)n_v(E)n_c'(E+\hbar\omega)dE}{\int_{E_{min}}^{E_{max}} M(E,\hbar\omega)n_v(E)n_c'(E+\hbar\omega)dE} \quad \ldots (9)$$

The $Q(\hbar\omega)$ term is unique to cathodoluminescence and is due to the fact that carrier generation by the electron beam also features in the detailed balance (i.e. $r_e(\hbar\omega)$ in Equation 5). From Equation (9) $Q(\hbar\omega)$ is the ratio of electron to photon transition rates across the band gap and is a positive quantity. If the transition matrix elements L and M show little variation over the energy range [$E_{\min}$, $E_{\max}$] then $Q \approx L/M$. The first term, $n_\gamma^{\max}$, of the photon density in Equation (8) is a Bose-Einstein distribution for a system with chemical potential μ_γ. It will be shown below that steady-state luminescence takes place for $\mu_\gamma < \hbar\omega$, and under these conditions the second term involving $Q(\hbar\omega)$ in Equation (8) is negative. $n_\gamma^{\max}$ is therefore an upper limit to the photon density. It is also the equilibrium photon density in the absence of carrier generation by the incident electron beam [16].

From the continuity equation the photon flux density (j) flowing in an arbitrary direction labelled '*x*' is given by:

$$\frac{dj}{dx} = \frac{1}{4}r_{sp} - (r_a - r_{st}) = \frac{1}{4}r_{sp} - \alpha j \quad \ldots (10)$$

where α is the absorption coefficient and is a function of the photon energy $\hbar\omega$. The factor of ¼ for the spontaneous emission term r_{sp} is due to Lambert's law and takes into account the photon flux emitted in a hemisphere in the direction of '*x*' [17]. Integrating Equation (10) over a slab of thickness d gives the photon flux density j_d emitted by the material [16]:

$$j_d(\hbar\omega) = \left[\frac{a(\hbar\omega)c}{4n(\hbar\omega)^3}\right]\frac{D_\gamma(\hbar\omega)}{\exp\left(\frac{\hbar\omega-\mu_\gamma}{kT}\right)-1} = \left[\frac{a(\hbar\omega)c}{4n(\hbar\omega)^3}\right]n_\gamma^{\max}(\hbar\omega)$$

… (11)

where c is the speed of light and $n(\hbar\omega)$ is the refractive index of the material. The absorptivity $a(\hbar\omega)$ for the slab is defined as:

$$a(\hbar\omega) = [1 - R(\hbar\omega)][1 - \exp(-\alpha(\hbar\omega)d)] \quad \text{… (12)}$$

where $R(\hbar\omega)$ is the reflectivity between the material and surrounding medium.

Equation (11) indicates that the steady-state CL emission rate is proportional to the maximum photon density n_γ^{max}, which increases exponentially with μ_γ (Equation 8). The physical origin of this effect is illustrated schematically in Figure 1. At low electron beam injection (Figure 1a) the electron and hole quasi-Fermi level separation μ_γ is small and consequently there are fewer electrons in the conduction band and holes in the valence band. The spontaneous emission rate will therefore be relatively low (Equation 1c). Furthermore, the photoabsorption rate will be larger than the stimulated emission rate (Equations 1a and 1b), which results in a positive absorption coefficient (Equation 10). The combined effects of a small spontaneous emission rate and net absorption gives rise to weak CL emission. The quasi-Fermi level separation however increases with electron beam injection (Figure 1b), meaning that CL emission is enhanced due to a higher spontaneous emission rate and somewhat smaller absorption coefficient. From Equation (8) n_γ^{max} is found to diverge when $\mu_\gamma = \hbar\omega$. This occurs when the absorption and stimulated emission rates are equal (Equation 6). For a semiconductor with equal electron and hole effective mass (or equivalently equal conduction and valence band effective density of states) n_γ^{max} diverges when the quasi-Fermi levels are aligned with the band edges and there are an equal number of occupied and unoccupied states in both conduction and valence bands (i.e. $n_v(E) = n_v'(E)$ and similarly for the conduction band). It should be noted that although n_γ^{max} diverges the absorption coefficient α and absorptivity a are zero, so that the CL emission rate still remains finite (Equations 11 and 12).

An interesting situation arises when the quasi-Fermi level splitting μ_γ is larger than the transition energy $\hbar\omega$. From Figure 1c this corresponds to a population inversion, where the bottom of the conduction band is now largely fully occupied and the top of the valence band is nearly empty. Although spontaneous and stimulated emission could still in principle take place, photoabsorption will be suppressed, so that a steady-state photon density cannot be maintained [16]. In fact n_γ has a physically unrealistic negative value under these conditions. For example, in the limit $(\mu_\gamma - \hbar\omega) >> kT$, n_γ^{max} is approximately $-D_\gamma(\hbar\omega)$ and the second term in Equation (8) tends to zero, so that $n_\gamma < 0$. For the material to be in steady-state then any electronic transition from the conduction to valence band must be via a non-radiative process, such as Auger recombination, while the incident electron beam must transfer sufficient energy to allow transitions from the valence to conduction band at an equal rate in order to maintain constant electron and hole concentrations (i.e. $r_e = r_{\text{Auger}}$; Equation 5). At these high carrier concentrations Auger recombination is also likely to be dominant over radiative recombination, since the cross-section for the former has a tri-molecular dependence compared to bi-molecular for the latter [27]. The band edge luminescence is therefore expected to increase monotonically with electron beam injection until the quasi-Fermi level separation becomes larger than the

band gap, at which point a population inversion occurs and steady-state luminescence is no longer possible.

The above concepts can be readily applied to discrete energy levels, such as those found in donor-acceptor pair (DAP) recombination. For DAP transitions the photoabsorption, stimulated and spontaneous emission rates are modified to:

$$r_a(\hbar\omega) = n_\gamma(\hbar\omega)M(\hbar\omega)N_A f_A(E_A)N_D[1 - f_D(E_D)] \quad \ldots (13a)$$

$$r_{st}(\hbar\omega) = n_\gamma(\hbar\omega)M(\hbar\omega)N_A[1 - f_A(E_A)]N_D f_D(E_D) \quad \ldots (13b)$$

$$r_{sp}(\hbar\omega) = D_\gamma(\hbar\omega)M(\hbar\omega)N_A[1 - f_A(E_A)]N_D f_D(E_D) \quad \ldots (13c)$$

The DAP transition energy $\hbar\omega$ includes a Coulomb interaction term that is a function of the spatial separation r of ionised donor and acceptor states [2]. Hence N_A, N_D are the number density of acceptor and donor states of spacing r respectively, and f_A, f_D are the corresponding electron occupation probabilities. For a *single* defect energy level E_T the occupation probability f_T is given by [27]:

$$f_T(E_T) = \frac{\sigma_{nT}n + \sigma_{pT}p_T}{\sigma_{nT}(n + n_T) + \sigma_{pT}(p + p_T)} \quad \ldots (14)$$

where σ_{nT}, σ_{pT} are the electron and hole capture cross-sections respectively. The conduction band electron (n) and valence band hole (p) concentrations are obtained using standard formulae [26]:

$$n = N_c \exp\left[-\frac{(E_c - E_{Fn})}{kT}\right] \;;\; p = N_v \exp\left[-\frac{(E_{Fp} - E_v)}{kT}\right] \quad \ldots (15)$$

with N_c, N_v being the effective density of states for the conduction and valence bands respectively. n_T and p_T follow from Equation (15) by setting the electron and hole quasi-Fermi levels equal to E_T. It is assumed that Equation (14) can be applied to the donor and acceptor states, which is a reasonable approximation provided that the separation r is sufficiently large. The notation T = A, D is used here to denote acceptor and donor states respectively. Using arguments outlined previously it is easy to show that the maximum photon density $n_\gamma^{\max}$ for the DAP transition is given by:

$$n_\gamma^{\max}(\hbar\omega) = \frac{D_\gamma(\hbar\omega)}{\left[\frac{f_A(E_A)}{1 - f_A(E_A)}\right]\left[\frac{1 - f_D(E_D)}{f_D(E_D)}\right] - 1} = \frac{D_\gamma(\hbar\omega)}{\left(\frac{\sigma_{nA}n + \sigma_{pA}p_A}{\sigma_{nA}n_A + \sigma_{pA}p}\right)\left(\frac{\sigma_{nD}n_D + \sigma_{pD}p}{\sigma_{nD}n + \sigma_{pD}p_D}\right) - 1} \quad \ldots (16)$$

The CL emission rate is obtained by substituting the above expression for n_γ^{max} in Equation (11).

Figure 2a calculates n_γ^{max} for DAP transitions in CdTe at 77 K (i.e. liquid nitrogen) temperature. The energy for donor and acceptor states is 0.1 eV; in this paper the donor and acceptor energies are measured with respect to the conduction band minimum and valence band maximum respectively. The cross-section ratios were taken as $(\sigma_{nD}/\sigma_{pD}) = 100$ and $(\sigma_{nA}/\sigma_{pA}) = 0.01$, along with values of $N_c = 8.0 \cdot 10^{17}$ cm^{-3} and $N_v = 1.8 \cdot 10^{19}$ cm^{-3} for CdTe [28]. For simplicity it is assumed that the donor, acceptor state concentrations are small, so that the electron (n) and hole (p) free carrier concentrations are due primarily to generation by the incident electron beam and therefore $n = p$. n_γ^{max} is plotted as a function of the free carrier concentration (i.e. n or p) on a logarithmic scale. From Equation (16) it is clear that the maximum photon density diverges when the denominator is equal to zero, or in other words when the value $\beta = [f_A(E_A)/\{1- f_A(E_A)\}]\cdot[\{1- f_D(E_D)\}/f_D(E_D)]$ is unity. The β-value is a function of the free carrier concentration and is superimposed in Figure 2a. Using the $\beta = 1$ criterion it can be deduced that photon divergence occurs at a free carrier concentration of ~10^{12} cm^{-3}. At higher carrier concentrations the β-value is less than unity and hence photon emission is not allowed. Figure 2a shows that at the point of photon divergence the electron quasi-Fermi level has a lower energy than the donor state. Under these high injection conditions, assuming $n >> n_D$, it follows that:

$$\frac{1 - f_D(E_D)}{f_D(E_D)} = \frac{\sigma_{nD} n_D + \sigma_{pD} p}{\sigma_{nD} n + \sigma_{pD} p_D} \approx \left(\frac{\sigma_{pD}}{\sigma_{nD}}\right) < 1 \quad \ldots (17)$$

In deriving Equation (17) the two relationships $n = p$ and $n_D > p_D$ have been made use of and it is reasonably assumed that the capture cross-section for an electron is larger than a hole due to the proximity of the donor level to the conduction band energy minimum. Similarly high injection (i.e. $p >> p_A$) for an acceptor state results in:

$$\frac{f_A(E_A)}{1 - f_A(E_A)} = \frac{\sigma_{nA} n + \sigma_{pA} p_A}{\sigma_{nA} n_A + \sigma_{pA} p} \approx \left(\frac{\sigma_{nA}}{\sigma_{pA}}\right) < 1 \quad \ldots (18)$$

Therefore if the electron, hole quasi-Fermi levels have lower energy than the donor, acceptor states, such that Equations (17) and (18) are satisfied, then the defect levels have effectively undergone a population inversion, meaning that steady-state DAP luminescence is not possible (from Equation (16) the value of n_γ^{max} becomes negative). This is similar to the conclusions for band edge luminescence discussed previously. However, it is not strictly necessary that both quasi-Fermi levels have lower energy than the corresponding defect states. The condition can be satisfied for only one quasi-Fermi level, but so long as the overall β-value is less than unity luminescence will still be suppressed. This is what is observed in Figure 2a where only the electron quasi-Fermi level has lower energy than the donor state at the point of photon divergence.

Figure 2b plots n_γ^{max} as a function of free carrier concentration for the case where the acceptor energy is 0.15 eV, while the donor energy is unchanged at 0.1 eV. All other parameters are the same as Figure 2a. The smaller DAP transition energy in Figure 2b is intended to simulate a scenario where the (ionised) donor-acceptor pair separation r is larger, so that the Coulomb interaction is less. Photon divergence occurs at lower free carrier concentration and hence electron beam injection compared to Figure 2a. At photon divergence only the hole quasi-Fermi level energy is less than the acceptor state energy. The lower injection is easily explained, since the condition $p >> p_A$ is easier to achieve when the acceptor energy is larger (i.e. 0.15 eV rather than 0.1 eV). A lower electron beam injection for photon divergence is also observed in Figure 2c where the DAP transition energy is the same as Figure 2b, but where the donor energy is now 0.15 eV and the acceptor energy is 0.1 eV. Here only the electron quasi-Fermi level energy is less than the donor state energy (i.e. $n >> n_D$) at the point of photon divergence. The variation of photon divergence with DAP transition energy and electron beam injection is consistent with experimental observations of blue shifting of the DAP peak for high injection conditions [2], i.e. at high injection DAP transitions of large r are suppressed (e.g. Figures 2b and 2c) leaving only the transitions corresponding to small r (e.g. Figure 2a).

3.2 *Experimental results*

Figure 3a shows room temperature CL spectra for CdTe acquired at 15 kV and variable incident beam currents. The total CL intensity in each spectrum has been normalised for a direct comparison. At the smallest electron beam current of 0.02 nA only a peak at ~951 nm is present. This peak has been attributed to native defects, such as dislocations, and becomes progressively weaker with chlorine doping [29]. Increasing the electron beam current to 0.1 nA results in the appearance of a band edge peak at 832 nm, which has been attributed to excitons as well as above band gap luminescence [30]. Higher electron beam currents increase the intensity of the 832 nm peak relative to that of the 951 nm peak. From section 3.1 luminescence is strongest when the quasi-Fermi level splitting is close to the energy of the radiative transition. On the other hand a quasi-Fermi level splitting larger than the radiative transition energy suppresses luminescence, since steady-state cannot be maintained. This is precisely what is observed in Figure 3a. At higher beam currents a greater fraction of the steady-state carrier distribution volume will have a quasi-Fermi level splitting larger than the 951 nm peak energy, meaning that its relative intensity decreases with respect to the (higher energy) 832 nm peak. Note that due to the non-uniform carrier generation by the electron beam, as well as surface recombination, the local quasi-Fermi level can vary within the material, and therefore it is possible to have CL spectra exhibiting both 832 nm and 951 nm peaks simultaneously.

The generalised radiation law can also be used to analyse spectral shapes. Consider the peak shape for band edge luminescence. The absorption coefficient is small for energies close to the band gap, so that from Equation (12) the absorptivity $a(\hbar\omega) \approx [1\text{-}R(\hbar\omega)]\alpha(\hbar\omega)d$. Using the measured CL signal $I(\hbar\omega)$ a modified CL intensity I_{mod} can be defined such that $I_{mod}(\hbar\omega) = I(\hbar\omega)[n(\hbar\omega)^3(1\text{-}R(\hbar\omega))^{-1}\alpha(\hbar\omega)^{-1}]$. The optical properties for CdTe [31] are used to calculate the refractive index $n(\hbar\omega)$, reflectivity $R(\hbar\omega)$ and absorption coefficient $\alpha(\hbar\omega)$. From Equation (11) a graph of I_{mod} vs. energy $\hbar\omega$ has the form $b/[\exp\{(\hbar\omega\text{-}\mu_\gamma)/kT\}\text{-}1]$, where b and μ_γ are constants that can be determined by least squares fitting. The results for 1 nA and 10 nA incident beam currents are shown in Figures 3b and 3c respectively. In each case a good fit to

the experimental data points is obtained with the best fit values for μ_γ being 1.43 eV and 1.46 eV respectively. These values are similar to the room temperature CdTe band gap of 1.47 eV [31], the condition for strong luminescence. The overall fit of the data along with a μ_γ-value that is close to the band gap energy validates the generalised radiation law, at least for the case of band edge luminescence.

The generalised radiation law has also been tested on CdTe at cryogenic 77 K temperature (Figure 3d) as well as GaN at room temperature (Figure 3e). For CdTe at 77 K apart from the 951 nm defect peak and band edge luminescence (blue shifted to 808 nm due to the lower temperature) there is a further broad DAP peak at ~890 nm [29]. The general trend is that with increasing incident beam current the relative intensity of the 951 nm defect peak is first suppressed, followed by a decrease of the DAP peak intensity with respect to the band edge peak, exactly as predicted by the generalised radiation law. The CL spectrum for GaN in Figure 3e consists of band edge luminescence as well as a broad 'yellow luminescence' peak centred around ~588 nm. The latter is thought to be a DAP transition between shallow impurity donors and deep cation vacancy acceptors [32-33]. The band edge luminescence consists of two peaks at 368 and 373 nm. The 368 nm peak has a long tail extending to energy values above the band gap and is therefore designated a band-to-band transition. The 373 nm peak could be exciton related [34], due to the small binding energy of 50 meV.

In GaN increasing the incident beam current tends to decrease the yellow luminescence intensity with respect to band edge luminescence, consistent with the generalised radiation law. However, more subtle effects are also observed. For example, the main yellow luminescence peak is 'suppressed' faster than the deep luminescence band between 706-738 nm, as most clearly seen in the CL spectrum acquired at 10 nA incident beam current (Figure 3e). From section 3.1 the yellow DAP luminescence will be suppressed at relatively low beam currents when the hole quasi-Fermi level energy becomes less than that of the deep acceptor [33]. The 706-738 nm luminescence band may involve electronic transitions between energy levels shallower than the yellow luminescence acceptor, but where the overall transition energy is smaller than yellow luminescence (recall that yellow luminescence has a shallow donor level at ~25 meV [32]). This could explain the experimental results and suggests that the transition energy is not always a reliable indicator for the evolution of a CL peak with respect to electron beam injection. Attempts were also made to verify the shape of the GaN band edge luminescence peak, similar to Figures 3b and 3c, using complex refractive index values for GaN [35]. The results for 10 nA incident beam current is shown in Figure 3f. The least squares fit to the experimental data is unsatisfactory, particularly at low energies. This could be due to overlap with the 373 nm peak. Nevertheless the best fit value for μ_γ was 3.17 eV, which is similar to the GaN band gap of 3.43 eV [34], as required.

3.3 *Comparison with time resolved cathodoluminescence*

Figure 4 shows time integrated CL spectra for CdTe acquired at 12 K specimen temperature and with the electron beam in continuous and pulsed illumination modes. Several peaks are identified, namely a neutral acceptor bound exciton peak (A^0X) at 779 nm, a 797 nm peak due to oxygen impurities that consists of a strongly overlapping electron to acceptor (eA^0) and donor-acceptor pair (DAP_1) transition, as well as a second donor-acceptor pair (DAP_2) peak

that is also observed at 77 K temperature (Figure 3d) [15]. The DAP_2 peak in the pulsed CL spectrum is blue shifted with respect to the continuous mode spectrum, indicating a higher overall power density and hence larger quasi-Fermi level splitting for the former. However, in pulsed mode the eA^0/DAP_1 and DAP_2 peaks are stronger than the higher energy A^0X peak, which is in contrast to the continuous CL spectrum, and contrary to the predictions of the generalised radiation law. This suggests that the radiation law is not applicable to pulsed CL spectra, which is not surprising since steady-state conditions are not found in pulsed illumination. In this section a framework for interpreting time resolved CL spectra is developed using concepts borrowed from the generalised radiation law.

The various stages of pulsed illumination are illustrated schematically in Figure 5 [36]. Before illumination the free electrons in the conduction band and holes in the valence band are assumed to be in equilibrium (Figure 5a), such that their distributions are determined by a single Fermi energy level and temperature. In the 'coherent' stage (Figure 5b) straight after pulsing the excess carriers are at a higher temperature than the initial carrier distribution. Collisions between carriers then take place rapidly and after a few picoseconds a 'hot' carrier distribution with higher temperature and individual quasi-Fermi level is established (Figure 5c). Since phonons are not involved there is no energy loss during this stage. Phonon scattering takes place subsequently and results in gradual thermalisation of the hot carrier distribution. Along with recombination equilibrium is eventually reached (Figure 5a), provided the pulse repeat duration is sufficiently long.

Consider recombination of the hot carrier distribution. The net recombination rate (R_{net}) between two energy levels separated by energy $\hbar\omega$ is given by:

$$R_{\text{net}}(\hbar\omega, t) = r_{sp}(\hbar\omega, t) + r_{st}(\hbar\omega, t) + r_{\text{non-rad}}(\hbar\omega, t) - r_a(\hbar\omega, t) \quad \ldots (19)$$

where $r_{\text{non-rad}}$ represents non-radiative recombination (e.g. Auger). The recombination rates are now a function of time t, since the carrier distribution and its temperature are dynamically evolving. Furthermore, unlike the steady-state case carrier generation by the electron beam is not applicable. For band edge recombination R_{net} is a function of the product of electron (n) and hole (p) concentrations at any given time [26], i.e.:

$$R_{\text{net}}(\hbar\omega, t) = B(t)[n(t)p(t) - n_i(t)^2] = B(t)n_i(t)^2 \left\{ \exp\left[\frac{\mu_\gamma(t)}{kT}\right] - 1 \right\} \quad \ldots (20)$$

where B is the bi-molecular recombination rate and n_i is the intrinsic carrier concentration [26]. B and n_i are functions of time, since they depend on the instantaneous temperature of the hot carrier distribution. At the early stages the quasi-Fermi level splitting μ_γ may be sufficiently large to create a population inversion. From Equations (19) and (20) however R_{net} will be positive, meaning that spontaneous and stimulated emission can take place, provided that non-radiative transitions are not dominant. This is in contrast to the steady-state case, where luminescence is suppressed for a population inversion.

An expression will now be derived for the photon density n_γ valid for pulsed illumination. From Equation (1) and the definition of the absorption coefficient α (Equation 10) the spontaneous emission rate (r_{sp}) can be expressed as [16]:

$$r_{sp}(\hbar\omega, t) = \frac{\alpha(\hbar\omega, t) c D_\gamma(\hbar\omega)}{n(\hbar\omega, t)\left\{\exp\left[\frac{\hbar\omega - \mu_\gamma(t)}{kT}\right] - 1\right\}} \quad \ldots (21)$$

The above result does not assume steady-state conditions and is therefore valid for pulsed illumination as well. Furthermore, from Equation (10) it follows that:

$$r_a(\hbar\omega, t) - r_{st}(\hbar\omega, t) = \alpha(\hbar\omega, t) j(t) = \alpha(\hbar\omega, t) n_\gamma(t)\left[\frac{c}{n(\hbar\omega, t)}\right] \quad \ldots (22)$$

Substituting Equations (20-22) in (19) and assuming negligible non-radiative recombination gives an expression for the photon density n_γ:

$$n_\gamma(t) = \frac{D_\gamma(\hbar\omega)}{\left\{\exp\left[\frac{\hbar\omega - \mu_\gamma(t)}{kT}\right] - 1\right\}} - \frac{B(t) n_i(t)^2 n(\hbar\omega, t)\left\{\exp\left[\frac{\mu_\gamma(t)}{kT}\right] - 1\right\}}{\alpha(\hbar\omega, t) c} \quad \ldots (23)$$

When $\mu_\gamma < \hbar\omega$ the second term in the above expression is negative since $\alpha > 0$. n_γ cannot therefore be larger than the first term which decreases exponentially with μ_γ. It follows that with pulsed illumination significant band edge luminescence only occurs until the quasi-Fermi level splitting decreases to approximately the energy of the emitted photons. Generalising the result to other radiative transitions could potentially explain some well-known luminescence phenomena, such as the red shifting of the donor-acceptor pair peak with increasing time in time resolved CL experiments [37].

Two further subtleties complicate the interpretation of time resolved CL spectra. The first is that the temporal evolution of $\mu_\gamma(t)$ is determined by the *total* recombination rate, which is the sum of $R_{net}(\hbar\omega)$ for *all* energies $\hbar\omega$. This means that $\mu_\gamma(t)$ is largely governed by the fastest recombination channel(s). Second kinetics of the radiative transition also plays a role. For example, in the case of the A^0X peak in Figure 4 the free excitons must first bind to a neutral acceptor. There will therefore be a time delay before the A^0X peak appears in the transient spectrum. If $\mu_\gamma(t)$ decreases significantly within this time delay then the A^0X peak may be suppressed all together. In fact the importance of the carrier distribution profile on the evolution of transient spectra has been highlighted in previous time resolved CL studies [37].

4. Conclusions

Planck's generalised radiation law is used to analyse continuous illumination mode CL spectra where the material is in steady-state. Using band edge and donor-acceptor pair transitions as an example the importance of the electron and hole quasi-Fermi levels on the CL spectrum is highlighted. In particular, steady-state luminescence is shown to be suppressed when the quasi-Fermi level energy drops below the transition energy level, thereby causing a population inversion. The well-known phenomenon of blue shifting of the donor-acceptor pair peak with injection density is consistent with this mechanism. The predictions are experimentally verified on CdTe and GaN, which are exemplar solar cell and light emitting diode materials respectively. CL spectra acquired under pulsed illumination, as found in time resolved CL, have also been analysed. Here it is found that luminescence can take place under population inversion conditions, which is likely to be prevalent during the initial stages of pulsing. Luminescence continues until the quasi-Fermi levels drop below the transition energy levels. This provides a simple framework for analysing transient spectra in time resolved CL, although complications due to simultaneously competing recombination channels and reaction kinetics must also be taken into account for a complete understanding.

5. Acknowledgements

BGM would like to thank Dr Jon Major and Prof Ken Durose (University of Liverpool, UK) for providing the CdTe sample. Thanks are also due to Drs David Gachet and Samuel Sonderegger of Attolight AG, Switzerland for acquiring the data shown in Figure 4.

References

[1] B.G. Yacobi, D.B. Holt, *Cathodoluminescence Microscopy of Inorganic Solids*, Plenum Press, New York, 1990.
[2] I. Pelant, J. Valenta, *Luminescence Spectroscopy of Semiconductors*, Oxford University Press, 2012.
[3] J. Nelayah, M. Kociak, O. Stéphan, F.J. García de Abajo, M. Tencé, L. Henrard, D. Taverna, I. Pastoriza-Santos, L.M. Liz-Marzán, C. Colliex, Mapping surface plasmons on a single metallic nanoparticle, *Nature Phys.* **3** (2007) 348.
[4] M. Kuttge, E.J.R. Vesseur, A.F. Koenderink, H.J. Lezec, H.A. Atwater, F. J. García de Abajo, A. Polman, Local density of states, spectrum and far-field interference of surface plasmon polaritons probed by cathodoluminescence, *Phys Rev B* **79** (2009) 113405.
[5] M.J. Romero, H. Du, G. Teeter, Y. Yan, M.M. Al-Jassim, Comparative study of the luminescence and intrinsic point defects in the kesterite Cu_2ZnSnS_4 and chalcopyrite $Cu(In,Ga)Se_2$ thin films used in photovoltaic applications, *Phys Rev B* **84** (2011) 165324.
[6] B.G. Mendis. L. Bowen, Q.Z. Jiang, A contactless method for measuring the recombination velocity of an individual grain boundary in thin-film photovoltaics, *Appl. Phys. Lett.* **97** (2010) 092112.
[7] B.G. Mendis, M.C.J. Goodman, J.D. Major, A.A. Taylor, K. Durose, D.P. Halliday, The role of secondary phase precipitation on grain boundary electrical activity in Cu_2ZnSnS_4 (CZTS) photovoltaic absorber layer material, *J. Appl. Phys.* **112** (2012) 124508.
[8] G. Stechmann, S. Zaefferer, T. Schwarz, P. Konijnenberg, D. Raabe, C. Gretener, L. Kranz, J. Perrenoud, S. Buecheler, A.N. Tiwari, A correlative investigation of grain boundary

crystallography and electronic properties in CdTe thin film solar cells, *Sol. Energy Mat. Sol. Cells* **166** (2017) 108.
[9] A.P. Levanyuk, V.V. Osipov, Edge luminescence of direct-gap semiconductors, *Usp. Fiz. Nauk* **133** (1981) 427.
[10] M.J. Romero, K. Ramanathan, M.A. Contreras, M.M. Al-Jassim, R. Noufi, P. Sheldon, Cathodoluminescence of Cu(In,Ga)Se_2 thin films used in high efficiency solar cells, *Appl. Phys. Lett.* **83** (2003) 4770.
[11] B.G. Mendis, A.A. Taylor, M. Guennou, D.M. Berg, M. Arasimowicz, S. Ahmed, H. Deligianni, P.J. Dale, Nanometre-scale optical property fluctuations in Cu_2ZnSnS_4 revealed by low temperature cathodoluminescence, *Sol. Energy Mat. Sol. Cells* **174** (2018) 65.
[12] M. Merano, S. Sonderegger, A. Crottini, S. Collin, P. Renucci, E. Pelucchi, A. Malko, M.H. Baier, E. Kapon, B. Deveaud, J.-D. Ganière, Probing carrier dynamics in nanostructures by picosecond cathodoluminescence, *Nature* **438** (2005) 479.
[13] S. Meuret, M. Solà Garcia, T. Coenen, E. Kieft, H. Zeijlemaker, M. Lätzel, S. Christiansen, S. Y. Wood, Y.H. Ra, Z. Mi, A. Polman, Complementary cathodoluminescence lifetime imaging configurations in a scanning electron microscope, *Ultramicroscopy* **197** (2019) 28.
[14] S. Sonderegger, E. Feltin, M. Merano, A. Crottini, J.F. Carlin, R. Sachot, B. Deveaud, N. Grandjean, J.D. Ganiere, High spatial resolution picosecond cathodoluminescence of InGaN quantum wells, *Appl. Phys. Lett.* **89** (2006) 232109.
[15] B.G. Mendis, D. Gachet, J.D. Major, K. Durose, Long lifetime hole traps at grain boundaries in CdTe thin-film photovoltaics, *Phys. Rev. Lett.* **115** (2015) 218701.
[16] P. Würfel, The chemical potential of radiation, *J. Phys. C: Solid State Phys.* **15** (1982) 3967.
[17] P. Würfel, *The Physics of Solar Cells*, Wiley-VCH, Weinheim, 2009.
[18] B. Feuerbacher, P. Würfel, Verification of a generalised Planck law by investigation of the emission from GaAs luminescent diodes, *J. Phys.: Condes. Matter* **2** (1990) 3803.
[19] K. Schick, E. Daub, S. Finkbeiner, P. Würfel, Verification of a generalised Planck law for luminescence radiation from silicon solar cells, *Appl. Phys. A* **54** (1992) 109.
[20] E. Daub, P. Würfel, Ultralow values of the absorption coefficient of Si obtained from luminescence, *Phys. Rev. Lett.* **74** (1995) 1020.
[21] J.K. Katahara, H.W. Hillhouse, Quasi-Fermi level splitting and sub-bandgap absorptivity from semiconductor luminescence, *J. Appl. Phys.* **116** (2014) 173504.
[22] G.H. Bauer, R. Brüggemann, S. Tardon, S. Vignoli, R. Kniese, Quasi-Fermi level splitting and identification of recombination losses from room temperature luminescence in Cu($In_{1-x}Ga_x$)Se_2 thin films versus optical band gap, *Thin Solid Films* **480-481** (2005) 410.
[23] G. El-Hajje, D. Ory, J.F. Guillemoles, L. Lombez, On the origin of the spatial inhomogeneity of photoluminescence in thin-film CIGS solar devices, *Appl. Phys. Lett.* **109** (2016) 022104.
[24] J.D. Major, Y.Y. Proskuryakov, K. Durose, G. Zoppi, I. Forbes, Control of grain size in sublimation-grown CdTe, and the improvement in performance of devices with systematically increased grain size, *Sol. Energy Mat. Sol. Cells* **94** (2010) 1107.
[25] M. Inokuti, Inelastic collisions of fast charged particles with atoms and molecules- the Bethe theory revisited, *Rev. Mod. Phys.* **43** (1971) 297.
[26] D.A. Neamen, *An Introduction to Semiconductor Devices*, McGraw-Hill, 2005.
[27] H.J. Möller, *Semiconductors for Solar Cells*, Artech House, Massachusetts, 1993.

[28] M. Gloeckler, A.L. Fahrenbruch, J.R. Sites, Numerical modelling of CIGS and CdTe solar cells: setting the baseline (2003) Proc. 3rd World Conference PVSEC, Osaka, Japan, pp.491-494.
[29] V. Consonni, G. Feuillet, S. Renet, Spectroscopic analysis of defects in chlorine doped polycrystalline CdTe, *J. Appl. Phys.* **99** (2006) 053502.
[30] J. Lee, N.C. Giles, D. Rajavel, C.J. Summers, Room temperature band-edge photoluminescence from cadmium telluride, *Phys. Rev. B* **49** (1994) 1668.
[31] D.A. Wood, K.D. Rogers, D.W. Lane, J.A. Coath, Optical and structural characterisation of CdS_xTe_{1-x} thin films for solar cell applications, *J. Phys.: Condens. Matter* **12** (2000) 4433.
[32] T. Ogino, M. Aoki, Mechanism of yellow luminescence in GaN, *Jpn. J. Appl. Phys.* **19** (1980) 2395.
[33] T. Mattila, R.M. Nieminen, Point-defect complexes and broadband luminescence in GaN and AlN, *Phys. Rev. B* **55** (1997) 9571.
[34] W. Liu, M.F. Li, S.J. Chua, GaN exciton photovoltaic spectra at room temperature, *Appl. Phys. Lett.* **71** (1997) 2511.
[35] T. Kawashima, H. Yoshikawa, S. Adachi, S. Fuke, K. Ohtsuka, Optical properties of hexagonal GaN, *J. Appl. Phys.* **82** (1997) 3528.
[36] M.A. Green, *Third Generation Photovoltaics: Advanced Solar Energy Conversion*, Springer, Berlin, 2003.
[37] D. Bimberg, H. Münzel, A. Steckenborn, J. Christen, Kinetics of relaxation and recombination of non-equilibrium carriers in GaAs: carrier capture by impurities, *Phys. Rev. B* **31** (1985) 7788.

Figures

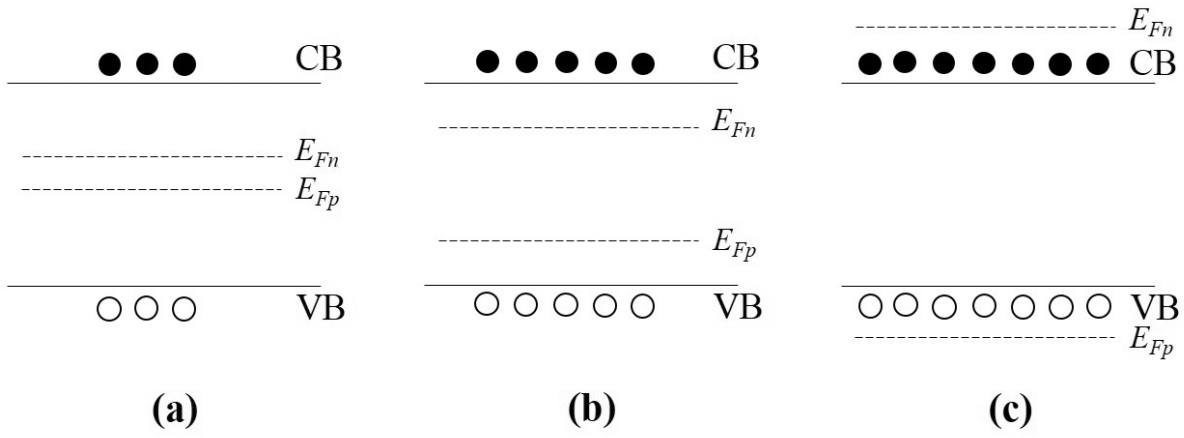

Figure 1: Schematic of electrons (solid circles) and holes (open circles) in the conduction (CB) and valence band (VB) respectively for different injection conditions. (a) shows low injection, where the electron (E_{Fn}) and hole (E_{Fp}) quasi-Fermi levels are closely spaced, so that the electron and hole concentrations are small, leading to weak luminescence. (b) shows high injection conditions. Here the quasi-Fermi level splitting is larger but still smaller than the band gap, and luminescence is consequently enhanced. (c) depicts a population inversion where steady-state luminescence is suppressed.

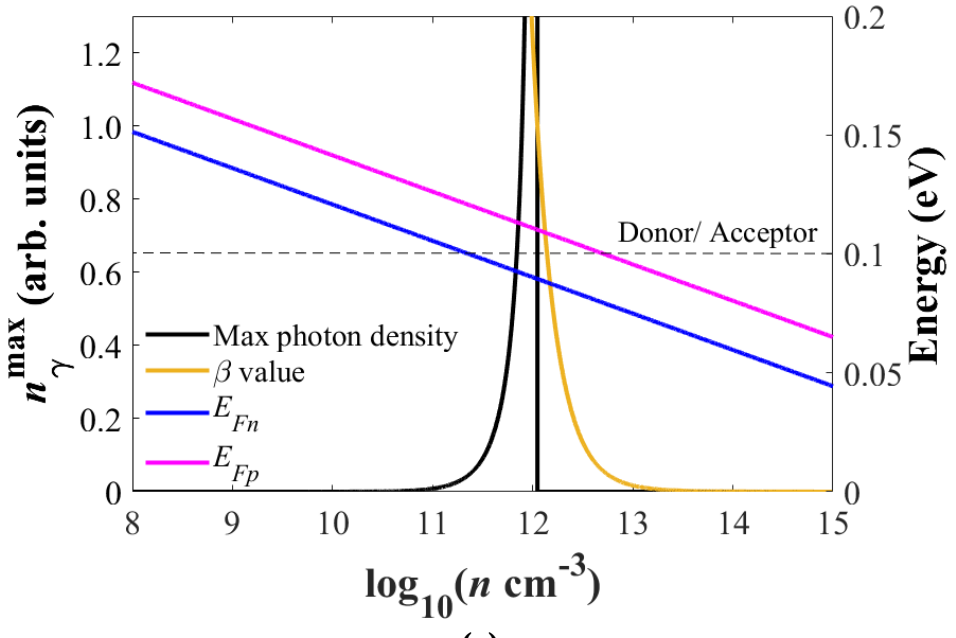
Max photon density
β value
E_{Fn}
E_{Fp}
Donor/ Acceptor
n_γ^{max} (arb. units)
Energy (eV)
$\log_{10}(n\ \mathrm{cm}^{-3})$

(a)

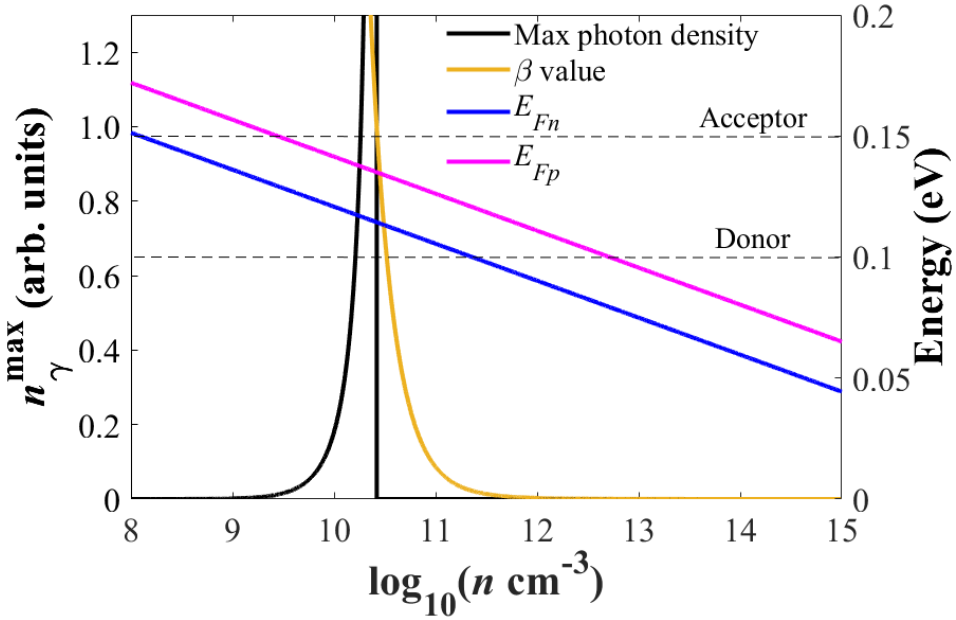
Max photon density
β value
E_{Fn}
E_{Fp}
Acceptor
Donor
n_γ^{max} (arb. units)
Energy (eV)
$\log_{10}(n\ \mathrm{cm}^{-3})$

(b)

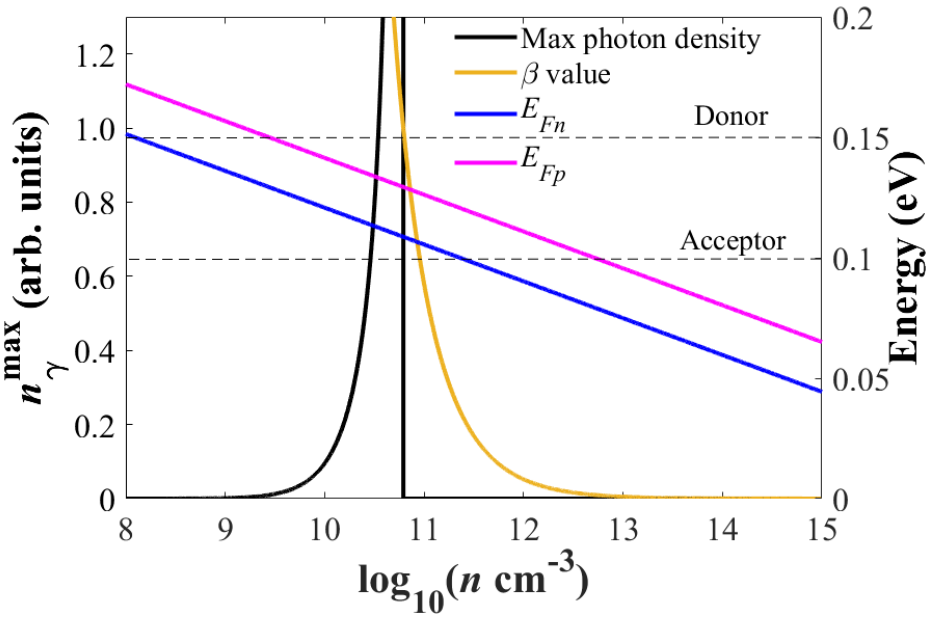

(c)

Figure 2: (a) Maximum photon density n_γ^{max} as a function of the logarithm of the free carrier concentration n (i.e. electrons or holes) for a donor-acceptor pair transition in CdTe at 77 K temperature. The donor and acceptor energies are 0.1 eV and the cross-section ratios are $(\sigma_{nD}/\sigma_{pD}) = 100$ and $(\sigma_{nA}/\sigma_{pA}) = 0.01$ respectively. Also shown are plots for the β-value, where $\beta = [f_A(E_A)/\{1-f_A(E_A)\}]\cdot[\{1-f_D(E_D)\}/f_D(E_D)]$, as well as the electron and hole quasi-Fermi levels E_{Fn} and E_{Fp}. The dashed horizontal line(s) represent the donor/acceptor state energy. The left hand vertical scale is used for plotting n_γ^{max} as well as the dimensionless β-value. The right hand vertical scale is used for plotting quasi-Fermi levels and defect state energies in eV. (b) is the equivalent plot for a 0.15 eV acceptor and 0.1 eV donor, while (c) is the equivalent plot for a 0.1 eV acceptor and 0.15 eV donor.

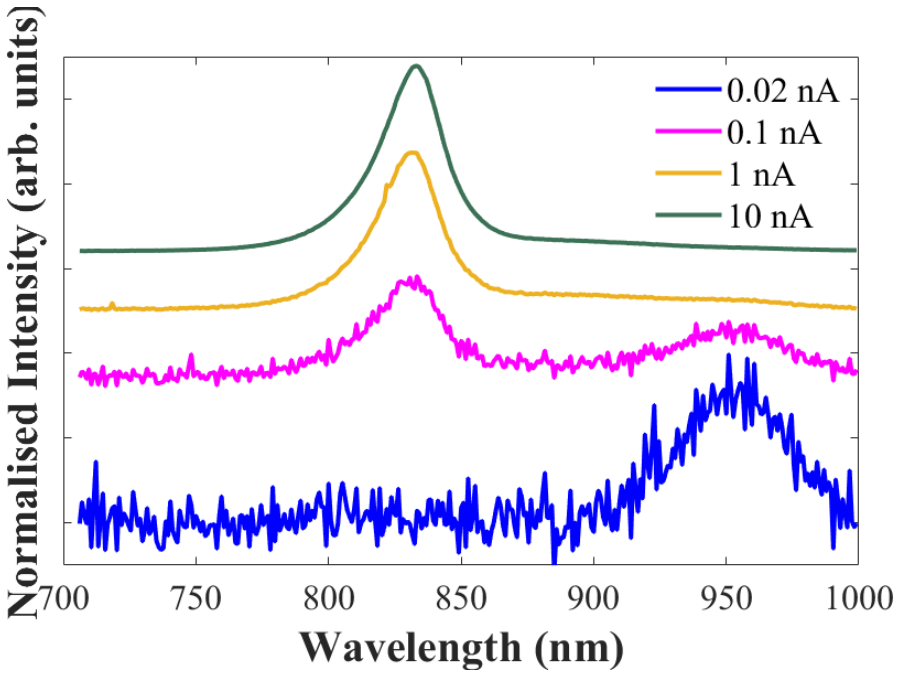

(a)

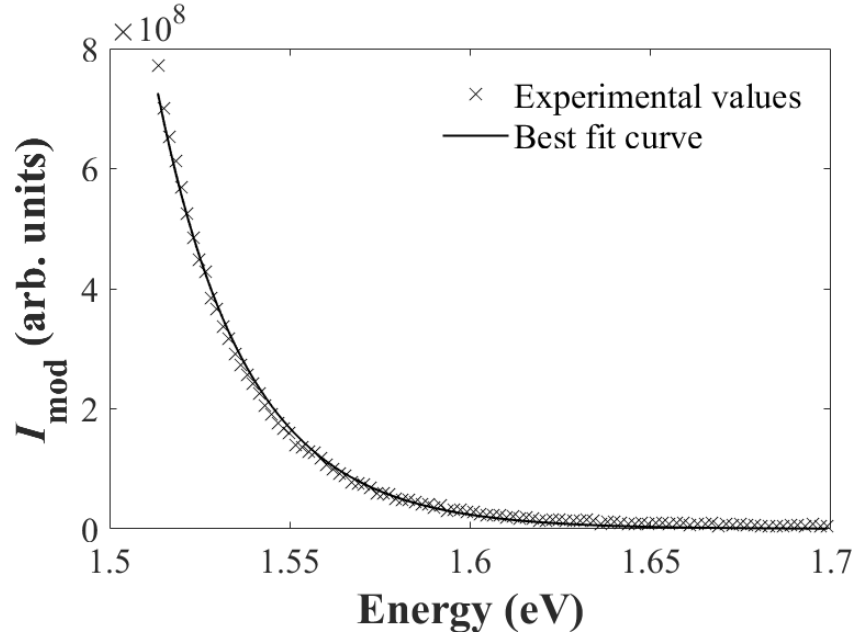
×10^8
8
6
4
2
0
1.5
1.55
1.6
1.65
1.7
Experimental values
Best fit curve
I_mod (arb. units)
Energy (eV)

(b)

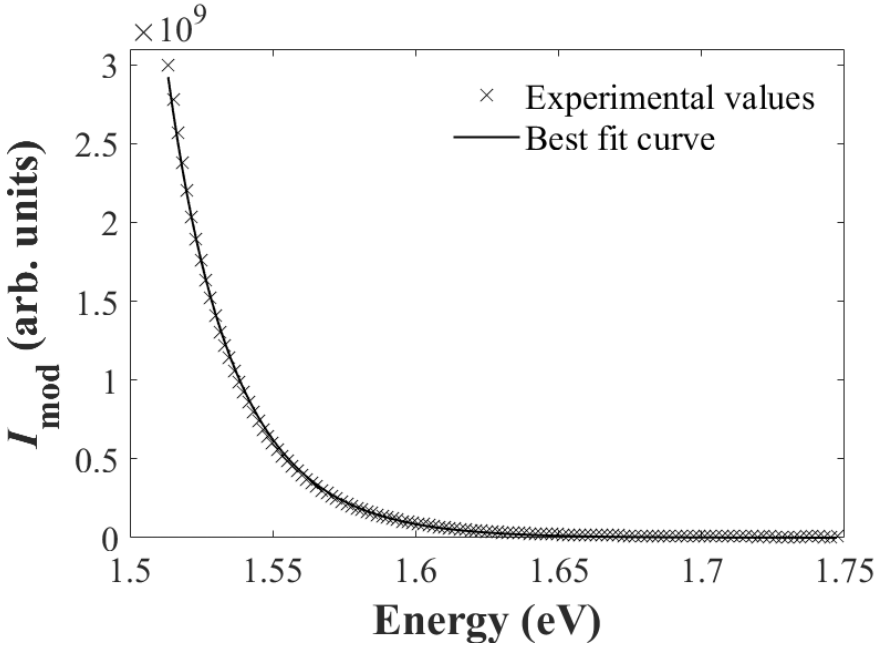
×10^9
3
2.5
2
1.5
1
0.5
0
1.5
1.55
1.6
1.65
1.7
1.75
Experimental values
Best fit curve
I_mod (arb. units)
Energy (eV)

(c)

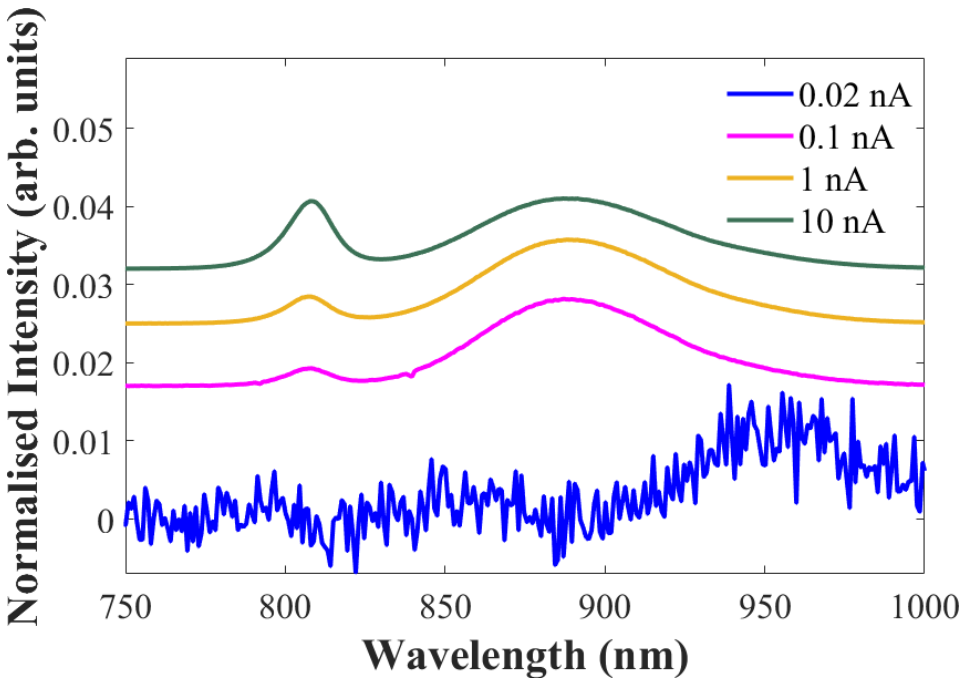
Normalised Intensity (arb. units)
0.05
0.04
0.03
0.02
0.01
0
750
800
850
900
950
1000
Wavelength (nm)
0.02 nA
0.1 nA
1 nA
10 nA

(d)

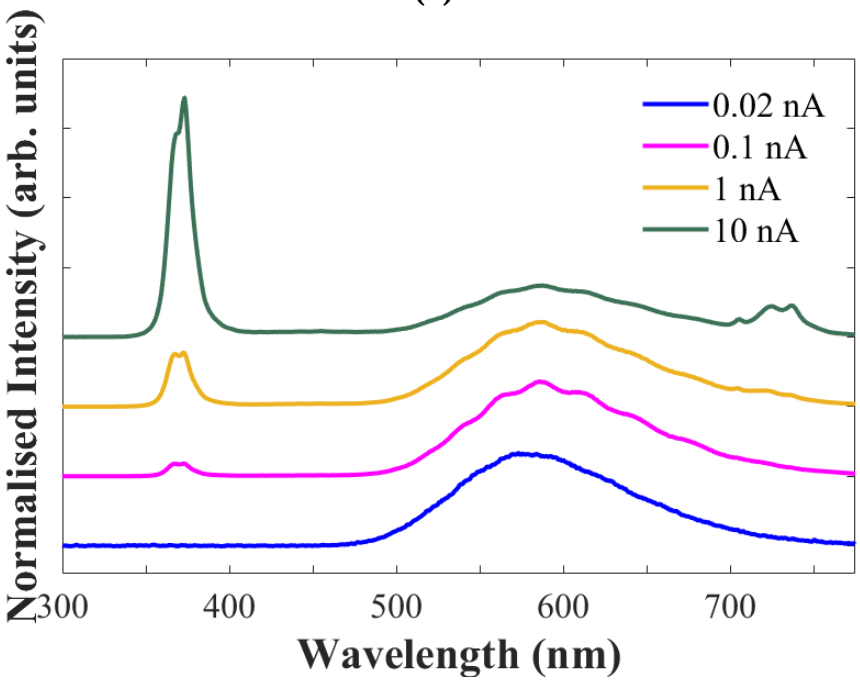
Normalised Intensity (arb. units)
300
400
500
600
700
Wavelength (nm)
0.02 nA
0.1 nA
1 nA
10 nA

(e)

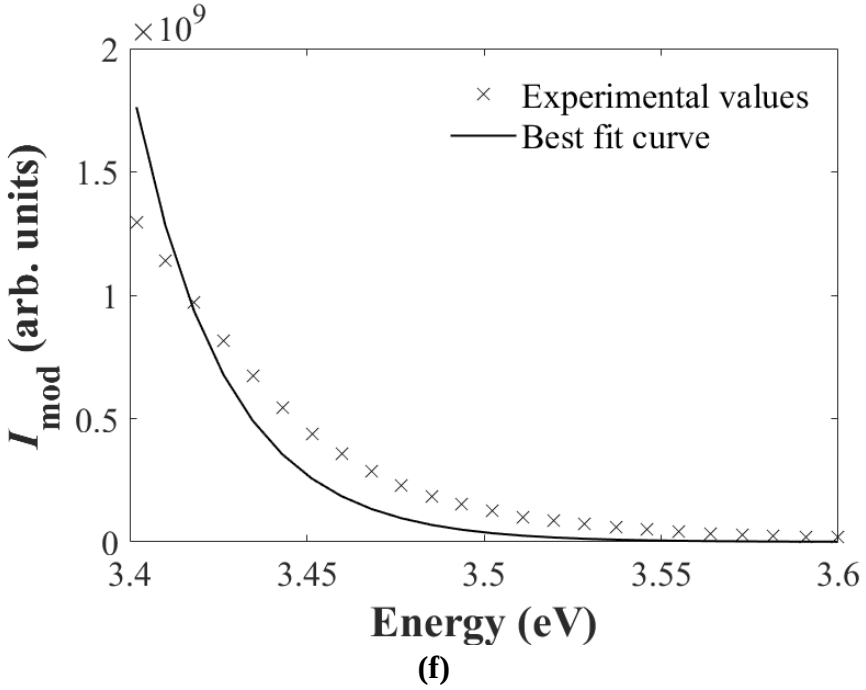

Figure 3: (a) Room temperature CdTe CL spectra as a function of incident electron beam current. The total intensity for each spectrum has been normalised and vertically shifted for clarity. (b) plots I_{mod} as a function of energy for band edge luminescence using data from the 1 nA room temperature CdTe spectrum (see text for further details). The equivalent plot for the 10 nA room temperature CdTe spectrum is shown in (c). (d) shows 77 K temperature, normalised CL spectra for CdTe as a function of incident electron beam current. Room temperature, normalised CL spectra for GaN as a function of incident electron beam current is shown in (e). (f) plots I_{mod} as a function of energy for band edge luminescence using data from the 10 nA room temperature GaN spectrum.

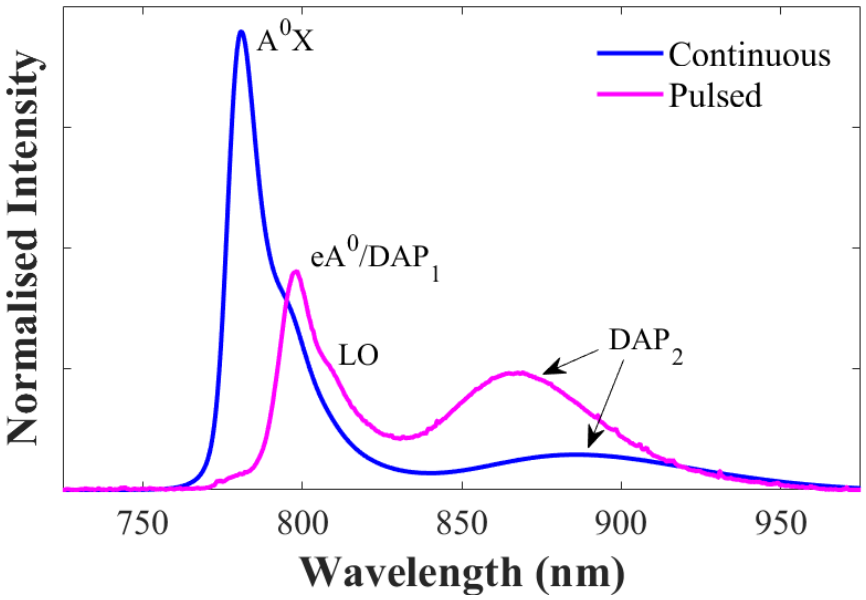

Figure 4: Time integrated CdTe CL spectra acquired in continuous and pulsed illumination modes at 12 K temperature. The total CL intensity has been normalised for direct comparison.

The A^0X, eA^0/DAP_1 and DAP_2 transitions are labelled (see text for further details). 'LO' denotes a phonon replica of the eA^0/DAP_1 peak.

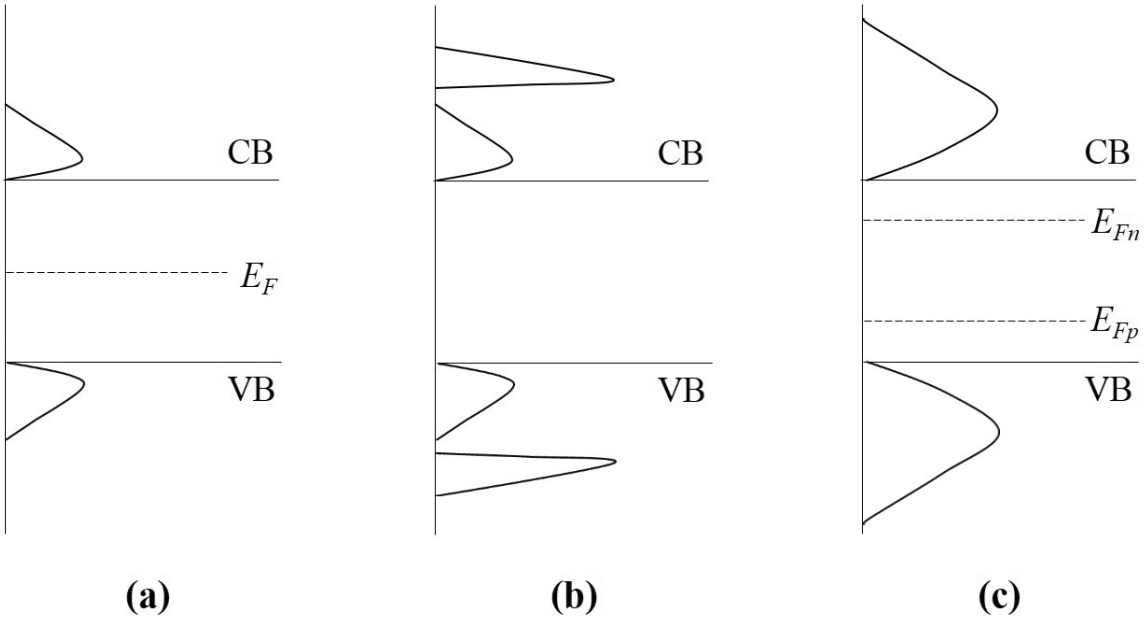

Figure 5: Electron and hole distributions in the conduction (CB) and valence (VB) bands at different stages of pulsed illumination. (a) shows the material before pulsing; carrier equilibrium is represented by a single Fermi level E_F. (b) is the so-called 'coherent' stage straight after pulsing, where the excess carriers generated by the pulse are superimposed on the equilibrium carrier distribution. In (c) the carriers have attained chemical and thermal equilibrium to form a 'hot' carrier distribution, defined by electron (E_{Fn}) and hole (E_{Fp}) quasi-Fermi levels. Figure adapted from reference [36].